Nanoscale

PAPER

View Article Online
View Journal | View Issue

Cite this: *Nanoscale*, 2020, **12**, 5898

Effect of a protein corona on the fibrinogen induced cellular oxidative stress of gold nanoparticles†

Inga Kuschnerus,[a,b] Michael Lau,[a] Kalpeshkumar Giri,[a,b] Nicholas Bedford,[c] Joanna Biazik,[d] Juanfang Ruan[d] and Alfonso Garcia-Bennett *[a,b]

The protein corona of nanoparticles is becoming a tool to understand the relation between intrinsic physicochemical properties and extrinsic biological behaviour. A diverse set of characterisation techniques such as transmission electron microscopy, mass spectrometry, dynamic light scattering, zeta-potential measurements and surface enhanced Raman spectroscopy are used to determine the composition and physical properties of the soft and hard corona formed around spherical gold nanoparticles. Advanced characterisation *via* small angle X-ray scattering and cryo-transmission electron microscopy suggests the presence of a thin hard corona of a few nm on 50 nm gold nanoparticles. The protein corona does not cause changes in cell viability, but inhibits the generation of reactive oxygen species in microglia cells. When a pre-incubated layer of fibrinogen, a protein with high affinity for the gold surface, is present around the nanoparticles before a protein corona is formed in bovine serum, the cellular uptake is significantly increased with an inhibition of ROS. The selective sequential pre-formation of protein complexes prior to incubation in cells is demonstrated as a viable method to alter the biological behaviour of nanoparticles.

Received 14th January 2020,
Accepted 7th February 2020

DOI: 10.1039/d0nr00371a

rsc.li/nanoscale

Introduction

Over the last decade, there has been a strong effort to control and understand the effects of protein opsonisation on the behaviour of nanoparticles (NPs) engineered for nanomedical applications in diagnostics and drug delivery applications. The corona that forms when nanoparticles come into contact with biological media is composed of a complex range of adsorbed biomolecules such as proteins, glycans and cytokines. This layer has been shown to mediate the basic biological process of administered particles such as cellular uptake, immunological response and toxicity, plasma circulation time and clearance.[1–3] Despite this, our understanding of how to control the physiological properties of NPs remains poor.

Among NPs being developed for medical imaging applications gold NPs (AuNPs) stand out due to the ease in which their optical properties can be tailored through surface plasmon resonance effects. Strong electromagnetic fields generated at the surface enhance the radiative properties allowing AuNPs to efficiently scatter light from the visible to near infrared, with small variations in particle size or aspect ratio.[4] This, in combination with their ability to accumulate passively in tumours or inflammation sites, and their ability to quickly convert absorbed light to heat *via* nonradioactive process makes them candidates for cancer photothermal therapies.[5] Understanding the protein corona (PC) of AuNPs may lead to new ways to direct and enhance their optical and biological properties.

The *in vivo* PC formed by AuNPs with different morphology were recently reported by Liz-Marzán *et al.*,[6] utilising intravenous injection. The NP were recovered after 10 min *via* a cardiac puncture. This work highlights the complexity of *in vitro* and *in vivo* PC characterisation, which may include changes to the morphology of the NPs during the incubation period in plasma. In terms of the protein composition, half of the proteins detected were present in all of the four NPs studied. Worth noting is the preference of low molecular weight proteins (<60 kDa) in the PC of AuNPs, mimicking results on liposomes, nanodiamonds and mesoporous silica particles.[7–9]

[a]*Dpt. Molecular Sciences, Macquarie University, Sydney, NSW, Australia. E-mail: alf.garcia@mq.edu.au*
[b]*Centre for Nanoscale and BioPhotonics, Macquarie University, Sydney, NSW, Australia*
[c]*School of Chemical Engineering, University of New South Wales, Sydney, NSW, Australia*
[d]*Electron Microscopy Unit, Mark Wainwright Analytical Centre, University of New South Wales, Sydney, NSW, Australia*

†Electronic supplementary information (ESI) available. See DOI: 10.1039/d0nr00371a

Functionalisation with polyethylene glycol (PEG) or aminopropylsilanes groups which hinders the hydrophobic and electrostatic interaction of high affinity proteins to the gold surface has been used as a strategy to inhibit the formation of a *hard* (and irreversible) PC on AuNPs.[9,10] The resulting loosely bound *soft* (and reversible) PC reduces the generation of reactive oxygen species (ROS) by the NPs in cellular assays. Thus pre-incubation with predesigned PCs prior to administration of NPs is an emerging strategy to direct their biological behaviour. McClements *et al.*, have shown using surface enhanced Raman spectroscopy (SERS) and transmission electron microscopy (TEM) that a stable AuNP–protein complex can be formed with β-lactoglobulin, a major globular protein present in bovine milk, which changes the colloidal stability of the NPs.[11] Similarly, Spinozzi *et al.* have studied the formation of AuNP–protein with serum albumin by *in situ* small angle X-ray scattering (SAXS) validating the corona formed as soft from a thermodynamic standpoint,[12] whereby one protein molecule of the gold surface moderately depresses the affinity for the association of other protein molecules.

In this work, the identification and characterisation of the hard *versus* soft PC of spherical AuNPs is tackled using a variety of *ex situ* techniques. The composition, size and surface charge differences of the PC of unfunctionalised AuNPs is measured at different bovine serum (BS) incubation times and with different washing steps to remove unbound proteins. Cryo-transmission electron microscopy (cryo-TEM) and SAXS indicate that a hard corona remains after prolonged incubation in BS, which affects the ability for these NPs to be taken up by microglia cells and to generate intracellular ROS. An enhancement of the nanoparticle uptake accompanied with an inhibition of ROS is observed when a pre-incubation step with fibrinogen (FIB), a high affinity protein for the gold surface prior to incubation in BS. The formation of AuNP–corona complexes *via* simple pre-incubation steps is shown to be a promising approach to alter and design the biological properties of AuNPs.

Experimental

Nanoparticles

AuNPs with a core size of 50 ± 3 nm, stabilised in 0.1 mM PBS suspension (Sigma Aldrich, Australia) were used for all experiments.

Protein corona preparation

400 μg AuNPs were incubated in 1 ml of BS for different times (10 min, 30 min, 120 min) at 22 °C. The hard corona was isolated *via* centrifugation for 15 min at 12 000 rpm at 4 °C. The supernatant was discarded and the remaining NP pellets redispersed in MilliQ water and either washed again or prepared for characterisation. Incubated NP samples were washed 1, 2 or 3 times after each incubation time. For the combined corona complexes AuNPs-FIB-BS and AuNPs-BS-FIB; AuNPs were incubated in FIB (2.5 mg ml^{-1} in MilliQ water) or BS for 60 min and washed 3 times. The AuNP–corona complex was then again incubated in BS (or FIB) for 60 min and washed 3 times.

For SERS measurement (see details below), the sample was further lyophilised overnight at 0.1 Pa and −50 °C. For characterisation by DLS, zeta-potential and cryo-TEM, the sample was diluted in MilliQ water.

Nanoparticle and protein corona characterisation

Dynamic light scattering (DLS) measurements were performed with a Zetasizer ZS (Malvern Instrument, UK) at 25 °C with a He–Ne laser (633 nm, 4 mW output power) as a light source. NP dispersions were measured in filtered PBS and again in filtered MilliQ water. The zeta-potential of the NPs was measured with a Zeta Sizer ZS (Malvern Instrument, UK) in filtered PBS and in filtered MilliQ water. Disposable folded capillary cells (Malvern Instrument, UK) were utilised.

For SERS, gold substrate microscope slides (Dynasil, USA) were used and prepared with approximately 1 mg of lyophilised sample. Measurements were immediately performed with a Sierra Raman Instrument (Snowy Range Instruments, USA) with a laser power of 30 mW, a wavelength of 785 nm and an integration time of 60 seconds. For each spectrum 10 measurements were recorded and averaged. Background measurements were obtained under the same condition as for the sample measurements and subtracted.

Prior to sample preparation for cryo-TEM, sample grids were treated with glow-discharge to make the carbon film hydrophilic. 4.5 μl of sample was placed onto a grid and any excess dispersion was removed by blotting with filter paper for 2.5 seconds. The grid was plunged into liquid ethane with a Leica EM GP freeze plunger (Leica, Germany) and stored in liquid nitrogen. Electron micrographs were obtained with a FEI Talos Arctica TEM (Thermo Fisher Scientific, USA) operating at 200 keV.

Proteomics

Gunshot proteomics was performed to extract molecular weight and isoelectric points of the proteins in the PC of AuNPs. AuNPs were mixed with 20 μL of lysis buffer and boiled for 5 min at 95 °C. The samples were further loaded in NUPAGE 4–12% BT GEL (Life Technologies), and the gel was run for 55–60 min at 200 mV in 20 times diluted MOPS SDS Running Buffer (10×, Thermo Scientific). Staining was performed with Coomassie Brilliant Blue R-250 Staining Solutions Kit (Bio-Rad) for 2 hours, followed by washing in MilliQ water for 2–3 days.

Small angle X-ray scattering

SAXS measurements were performed at the Small Angle/Wide Angle X-ray beamline of the Australian Synchrotron. The energy of the incident X-ray beam was set at 12 keV and the beam size was 250 μm horizontal ×450 μm vertical. The maximum flux at the samples was 8×10^{12} photons per second. The SAXS data were recorded by a 2D Dectris-Pilatus 200 K detector, positioned at 2.68 m from the sample.

Background scattering of the solvent and the experimental setup was subtracted from data.

Cell cultures

Immortalised murine microglia cells (BV2) were kindly donated by Dr Lindsay Parker (Macquarie University, Centre for Nanoscale Biophotonics, Australia). Microglia were cultured in DMEM supplemented with 10% FBS and 1% Penicillin/Streptomycin at 37 °C with 5% CO_2, 95% fresh air, and passaged every 3–4 days. Cells of passage between 10–15 days were used for the *in vitro* cell experiments outlined below.

In vitro cell experiments

Microglia were seeded onto 6 well plates at a density of 1 × 106 to 2 × 106 containing 2 ml cell culture media. Samples containing AuNPs (26 μg ml^{-1}) were incubated with the cells at 37 °C with 5% CO_2, 95% fresh air for 24 hours. Cellular oxidative stress, cell death and viability were analysed using a Muse® oxidative stress kit, and Muse™ count and viability kit, respectively. The Muse® oxidative stress kit determines the percentage of cells that are under oxidative stress (%ROS(+)) based on the intracellular detection of superoxide radicals, from cells that are not under oxidative stress (%ROS(−)). Each sample was analysed according to the protocol provided by the manufacturer. Briefly, media was removed from the six well plates, and TrypLE was used as the dissociation agent to recover the cells. Media was removed, and PBS was added to re-suspend the cell pellet. Data analysis was performed on the MUSE cell analyzer®.

The Muse™ count and viability reagent contain a DNA-binding dye that stains the nucleus of dead and dying cells. The dye does not stain live cells, allowing for the discrimination between dead and viable (live) cells. Samples were analysed following the protocols provided by the manufacturer. Briefly, media was removed from the six well plates, and TrypLE was used as the dissociation agent. Approximately 1 ml of fresh media was added to stop the TrypLE reaction and the cell suspension was added into 15 ml falcon tubes for centrifugation at 300 g for 3 min. Media was removed, and PBS was added to re-suspend the cell pellet. 10 μl of cell suspension was added to 400 μl of Muse™ count and viability reagent and incubated for 10 min. Data analysis was performed on the MUSE cell analyzer® containing the Muse™ count and viability software module that performs the calculations to determine the percentage of viable and dead cells.

Flow cytometry

The cellular uptake of AuNPs was quantified by flow cytometry (CytoFLEXS, Beckman Coulter, Australia). BV2 cells were grown on 24 well plates with a seeding density of 200 000 cells per ml at 37 °C, 5% CO_2, and 95% fresh air. AuNPs samples in cell culture media (DMEM supplemented with 10% FBS) were incubated with the BV2 cells for 16 and 24 hours. After the incubation time, BV2 cells were washed with PBS, detached with TrypLE express dissociation reagent, and centrifuged at 500 rpm for 5 min to remove the supernatant. Samples were resuspended in PBS for the fluorescent detection of AuNPs by the flow cytometer.[13] Ten thousand events were collected for each sample and the results were analysed using the CytExpert software (Beckman Coulter).

Biological electron microscopy

Prior to visualising the cell uptake of AuNPs in microglia the cells were grown on glass to 70–80% confluency. After the cell uptake, cell culture media was removed from the wells before slowly adding 1 ml fixative consisting of 2.5% glutaraldehyde and 1 mg ml^{-1} ruthenium red in 0.2 M Na cacodylate buffer. Fixation was started at room temperature and then cells were placed in the fridge (4 °C) overnight. After washing in MilliQ water, cells were postfixed in 1% OsO_4 in 0.1 M sodium cacodylate buffer using a BioWave Pro + Microwave Tissue Processor (Ted Pella, Inc., USA), washed again in MilliQ water, dehydrated with a graded series of ethanol, infiltrated with resin (Epon, LX112) and polymerised at 60 °C overnight. Ultrathin sections (70 nm) were collected onto carbon coated copper TEM grids, post stained with uranyl acetate (2%) and viewed using FEI Tecnai G2 20 TEM (Thermo Fisher Scientific, USA) electron microscope.

Results and discussion

AuNPs were commercially purchased reactant free and stabilised in 0.1 mM PBS, with an average core size of 50 nm and facetted morphologies (Fig. 1(a)). AuNPs were incubated with bovine serum (BS) at different incubation times: between 10–120 min (T_{10}, T_{30} or T_{120}). Samples were submitted to three washing cycles (W_{1-3}) in order to remove loosely bound proteins. The resulting AuNP–corona complexes are denoted by their incubation time and number of washing cycles.

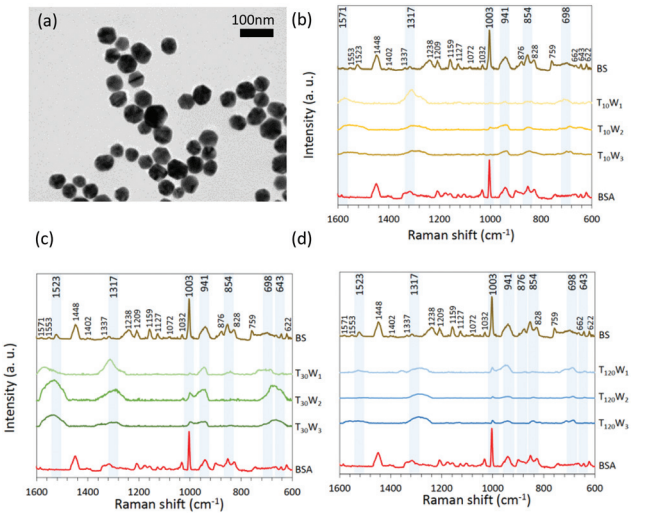

Fig. 1 Representative TEM image of AuNPs in the absence of a PC (a). SERS of AuNPs after incubation in BS at different incubation times and washing cycles to remove unbound proteins (b, c and d). The spectra of free BSA is shown for comparison.

Impact of the incubation time on physico-chemical properties

The SERS spectra of lyophilised solid samples of AuNPs as a function BS incubation time and number of washing cycles are shown in Fig. 1(b, c and d). The spectra of AuNPs without proteins (Fig. S1†), in the ESI† show bands that can be assigned to the adsorption of phosphate anions from the stabilising buffer, onto the gold surface.[14] Similarly, the SERS spectra of pure BS and FIB (Fig. S1†) shows characteristic bands consistent with previous reports.[15,16] Table S1† provides the tentative assignments of bands in the spectra of all AuNP–corona complexes. Albumin (BSA) is the most abundant protein in BS making up over 50% of the protein content, with approximately 24% of amino acid residues in BSA comprised of glutamic and aspartic acid (Glu and ASP), and 3.5% from phenylalanine (Phe).[17] The strong band at 1448 cm^{-1} corresponds to the CH_2 stretching vibrations, whilst bands associated with symmetric stretching modes of carboxyl groups at 1402 cm^{-1} are weak but discernible. The sharp and strong band at 1003 cm^{-1} (asymmetric ring breathing) is attributed to Phe residues. Bands between 800–900 cm^{-1} are consistent with aromatic residues of tyrosine (Tyr) and the bands at 698 cm^{-1} with the COO– deformation from Glu and Asp.[18] Another feature of the BS spectra is the presence of slightly broadened bands at 1238 cm^{-1} and 941 cm^{-1} corresponding to the helical chain amide-III regions and C–C bond stretching vibrations, respectively. The SERS spectra of BS incubated particles show peak broadening, consistent with significant conformational changes to proteins in the PC. Similar spectral features are observed at all incubation times. Interestingly, the broad bands between 1500–1600 cm^{-1} differ in intensity with washing cycles and incubation time. For example, the band at 1571 cm^{-1} (imidazole ring of C=C, C=N bonds), disappears completely at T_{120}. The amide II band and ring stretching of tryptophan (Tryp) at 1553cm^{-1} is only present for $T_{10}W_{2-3}$, $T_{30}W_{1-3}$. Only after removal of the loosely bound proteins does the NH_3^+ deformation band of lysine (Lys) at 1523 cm^{-1} appear in $T_{10}W_{2-3}$, $T_{30}W_{2-3}$, whereas after 120 min incubation it is also visible in the soft and hard PC ($T_{120}W_1$ and $T_{120}W_3$).

Overall, the intensity of SERS bands for samples incubated at T_{120} are less affected by washing cycles than those at the shorter incubation times. This is noticeable for the band at 1317 cm^{-1} (CH_2 twisting and bending) that rapidly decreases in intensity with washing steps at T_{10} and T_{30}, as proteins are removed from the PC. The 1003cm^{-1} (Phe) remains present for all incubated particles except for $T_{10}W_3$ where the peak is no longer visible suggesting a preferential depletion of albumin with washing cycles at T_{10}, but a stronger affinity with longer incubation time.

DLS measurements recorded after incubation in BS show an increase in the particle size of hard PC (W_3) of AuNPs with longer incubation time, with values increasing from 60 nm AuNPs to 243 nm at $T_{120}W_3$ (Fig. 2(a)). Particle size values decreases significantly with washing cycles suggesting that specific protein layers are removed resulting in a lower degree of agglomeration. Zeta-potential measurements show a

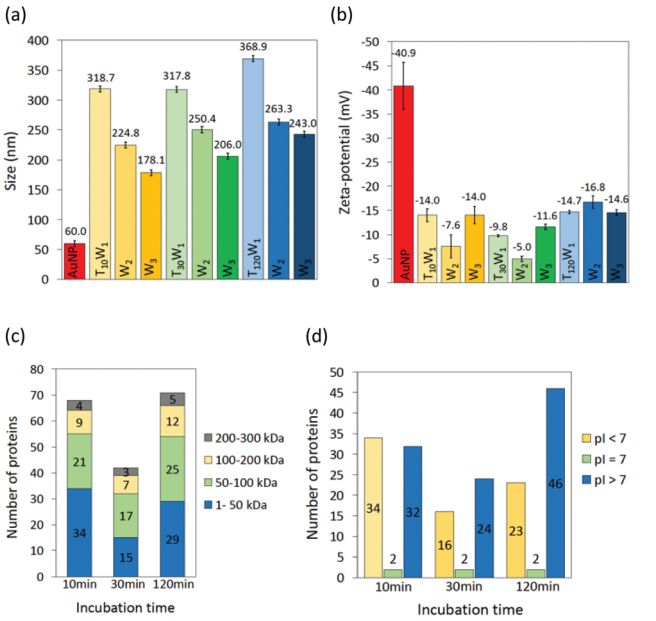

Fig. 2 Effect of PC washing cycles on (a) the particle size in water and (b) net surface charge (zeta-potential) in water of AuNPs after incubation at different times in BS. (c) Molecular weight distribution and (d) isoelectric point of proteins detected in the hard corona of AuNPs $T_{10}W_3$, $T_{30}W_3$ and $T_{120}W_3$.

decrease in surface charge (Fig. 2(b)), from approximately −41 mV to approximately −13 mV, for AuNPs incubated at all-time points and washed 3 times. The decrease in surface charge correlates well with previous published data by Dobrovolskaia *et al.*,[19] where a decrease in the net surface charge (less negative) of 30 nm AuNPs incubated in human plasma is accounted for by a sequential binding of (firstly) *cationic* proteins followed by *anionic* proteins. The observed fluctuations with different washing cycles agrees with this hypothesis, whereby protein layers are sequentially stripped revealing either a more neutral or more negative surface after W_2 and W_3 respectively, for T_{10} or T_{30}. At T_{120} the net surface charge increases after W_2, suggesting a different compositional makeup of the PC.

In order to confirm the different composition of the hard PC of AuNPs at different BS incubation time, proteomics analysis by mass spectrometry was conducted on samples $T_{10}W_3$, $T_{30}W_3$ and $T_{120}W_3$. A summary of the molecular weight and theoretical isoelectric point of the proteins detected for each sample is shown in Fig. 2(c and d). The size distribution of proteins initially decreases at T_{30} and subsequently increases at T_{120}. Similarly, the total number anionic proteins initially decrease only to subsequently increase at T_{120}, in agreement with the zeta-potential values. Analysis of detected proteins by their function (Fig. S2(a)†) reveals that the most abundant proteins in the hard PC of AuNPs incubated with BS (T_xW_3) is either of the *binding* and *structural molecule activity* type. Additionally, the $T_{120}W_3$–corona complex showed the highest similarity in the composition of proteins to free BS, with

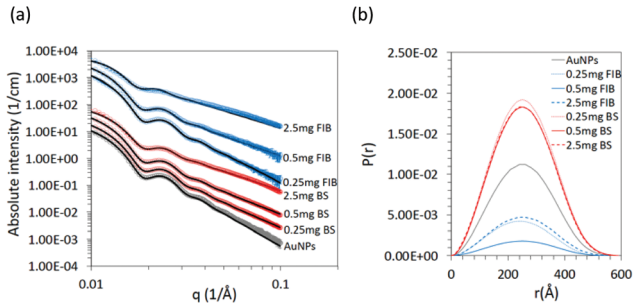

Fig. 3 (a) Background subtracted SAXS curves of pure 0.02 mg ml^{-1} AuNPs, AuNPs with BS and AuNPs and FIB at different concentrations (0.25 mg–2.5 mg ml^{-1}). Black curves represent the form factor fitting. Curves are scaled for better understanding. (b) Pair distance distribution function of AuNP–corona complexes obtained with the software ScÅtter.

approximately 13% correspondence in protein composition (Fig. S2(b)†).

The formation of a hard PC around the surface of AuNPs may be followed by measuring changes to the electron density and scattering contrast of the sample in solution. Fig. 3(a) shows SAXS measurements of pure AuNPs dispersed in water alone and at different concentrations of BS and FIB and their form factor fitting. The formation of a PC at different concentrations of BS and FIB affects the scattering in the higher q-range (0.05–0.1 Å^{-1}) by overshadowing the scattering peak of the AuNPs core. Agglomeration of both AuNPs–corona complexes is visible for the highest concentration (2.5 mg ml^{-1}) in the low q-range (0.01–0.012 Å^{-1}).

The best fit for the form factor is obtained with a Gaussian distribution of a core–shell spheroid. Due to less agglomeration, the best fitting results were obtained for 0.25 mg ml^{-1} BS with a mean core radius R_C = 24.810 nm and a shell thickness of D_S = 1.804 nm. The fitting results for the 0.25 mg ml^{-1} FIB reveal a similar mean core radius R_C = 24.538 nm, albeit with almost double the shell thickness, D_S = 3.175 nm. The accuracy of the fitting is decreased with increasing protein concentration. Additional fitting data can be found in Table S3.†

The pair distance distribution function (PDDF) was extracted (using the software ScÅtter‡) which provides model-independent information on the distance between pairs of particles in real space.[20] For spherical particles the PDDF shows a bell shape curve shown in Fig. 3(b). Table S2† lists the values of the D_{max} extracted from the PDDF. An increase in the particle radius between 1–2 nm (associated with the hard PC formation) is only visible at 0.25 mg ml^{-1} and 0.5 mg ml^{-1} BS concentration.

Cryo-TEM images confirm that the PC of AuNPs at $T_{120}W_3$ formed with BS or FIB has significantly different morphology and contrast features (Fig. 4). Control cryo-TEM images of pure

‡ScÅtter is a JAVA-based application for analysis of SAXS datasets. ScÅtter is developed by Robert Rambo at the Diamond Light Source (Didcot, UK). The program can be downloaded free of charge at http://www.bioisis.net.

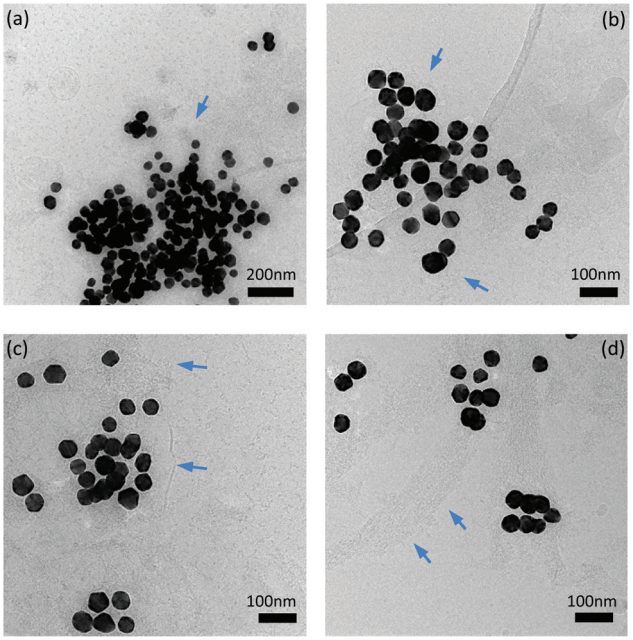

Fig. 4 Representative cryo-TEM images recorded on samples of AuNPs incubated at (a) $T_{120}W_1$ with BS (b) $T_{120}W_3$ with BS; (c) $T_{120}W_3$ with FIB and (d) $T_{120}W_3$ with FIB followed by BS. The PC is faintly visible on all images and is highlighted by arrows. Samples containing FIB and BS show evidence of fibre formation on the PC.

BS and FIB, and FIB-BS as well as additional micrographs of AuNP–corona complexes can be found in Fig. S4.† AuNPs are more prominent to agglomeration in the presence of BS. Evidence of the formation of fibrous structures are visible in the FIB PC of AuNPs (Fig. 4(c)) which is consistent with previous studies of its self-assembly and its known function as a blood clotting agent.[21] When adsorbed to AuNPs–COOH, FIB may adopt both side-on and end-on configurations depending on size, with 65 nm particles causing FIB to lose its secondary structure.[22] Interestingly, when a FIB AuNP–corona complex is first formed ($T_{60}W_3$) followed by a second incubation in BS ($T_{60}W_3$), the PC retains its fibrous morphology with a thicker fibre dimension as shown in Fig. 4(d). The average particle size of the AuNP-FIB-BS complex as measured by DLS (Fig. S5(a)†) also shows considerable agglomeration as a function of washing step due to the formation of FIB fibres. The zeta-potential behaviour of AuNP–corona complexes is characterised by being predominantly negative, albeit close to zero, indicating a high degree of agglomeration for these complexes (Fig. S5(b)†).

Different AuNP–corona complexes, including those formed *via* sequential incubations with different proteins, may lead to different biological outcomes in comparison to PC-free AuNPs. In order to explore their biological properties of in this context, AuNPs (26 μg ml^{-1}) were incubated with microglia cells (BV2) for 24 hours and levels of cell death, viability, cellular oxidative stress and cell uptake were measured (Fig. 5(a, b and c)). Neither the AuNPs alone nor the different AuNP–corona complexes influenced significantly the viability of the

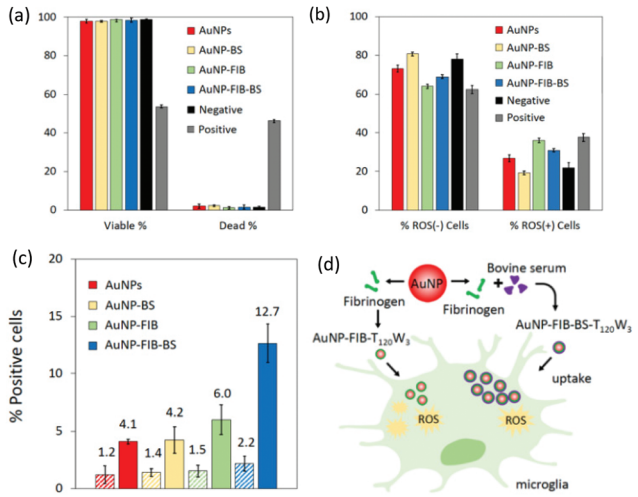

Fig. 5 (a) Cell death and viability of microglia cells incubated with AuNPs and preformed AuNPs–corona complexes for 24 hours. The negative control represents was microglia without NPs and the positive control microglia cells incubated with hydrogen peroxide (500 μM). (b) Microglia under oxidative stress (ROS(+)) expressed as a percentage compared to normal cells (ROS(−)) after 24 hours incubation, based on the intracellular detection of superoxide anion. (c) Flow cytometry analysis of AuNP–corona complex uptake by microglia after incubation for 16 (pattern bar) and 24 hours (solid bar) at 37 °C. Quantification of cellular uptake is based on the average value of three independent experiments ± S.D. (d) Schematic diagram of the effect of different AuNP–corona complexes.

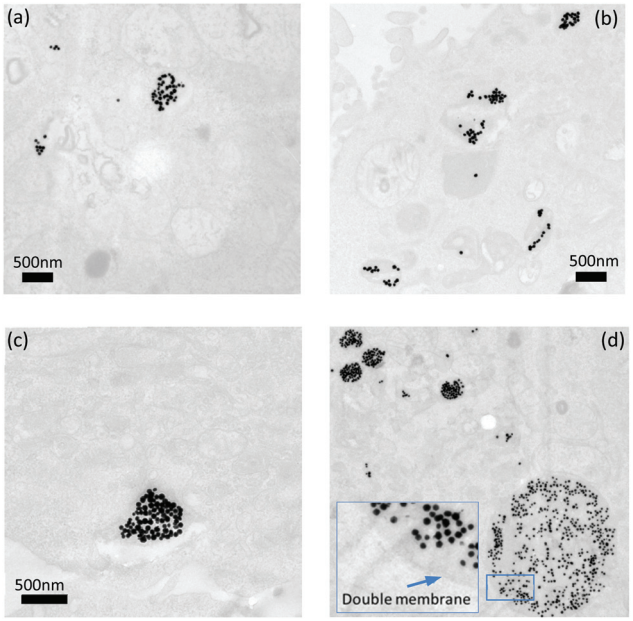

Fig. 6 Electron micrographs visualising cell uptake of AuNP–corona complexes in microglia cells after 24 hours. (a) Pure AuNPs without PC. (b) AuNPs with BS-$T_{120}W_3$ PC. (c) AuNPs with FIB-$T_{120}W_3$ PC. (d) AuNPs with FIB-BS-$T_{120}W_3$ PC. Image recorded (d) is recorded at the same magnification as that shown in (a).

cells in comparison to controls. The BS-$T_{120}W_3$ PC shows the lowest ROS(+) amount (20%), lower than for AuNPs alone. AuNPs with a FIB-$T_{120}W_3$ PC show the highest generation of intracellular oxidative stress with *ca.* 38% of ROS(+) cells (Fig. 5(b)); equivalent to a hydrogen peroxide solution at a concentration of 500 μM (positive control). FIB is reported to induce a 5 fold increases in H_2O_2 gene expression and contribute to ROS generation in inflammatory responses in microglia.[23]

Interestingly, when a FIB-$T_{60}W_3$ PC is first formed and particles subsequently incubated in BS for a further 60 min (FIB-BS-$T_{120}W_3$) the percentage of ROS(+) cells decreased in comparison to the FIB-$T_{120}W_3$.

The uptake of AuNPs by microglia cells was quantified by flow cytometry detection after 16 hours and 24 hours (Fig. 5(c)). An increase in cell uptake after 24 hours from 4.1% for pure AuNPs to 6.0% and 12.7% for AuNPs with a FIB-$T_{120}W_3$ and a combined FIB-BS-$T_{120}W_3$ hard corona respectively, is observed.

Pre-formation of a BS hard corona (BS-$T_{120}W_3$) does not lead to a significant increase in uptake in comparison to pure AuNPs. The significantly higher cell uptake for the FIB-BS corona complex is also evident from TEM (Fig. 6). In Fig. 6(a) uptake for pure AuNPs after 24 hours is clearly observed as AuNPs accumulate in late endosome and lysosome compartments. Fig. 6(b and c) show a similar cell uptake to Fig. 6(a). Fig. 6(d) shows a large double membraned autophagosome and four small lysosomes involved in the uptake of AuNPs with a FIB-BS-$T_{120}W_3$ PC. Qualitatively, a larger uptake is observed, and particles appear to cluster in greater numbers in comparison to other AuNP–corona complexes. The formation of large autophagosomes may be indicative of extracellular AuNP agglomeration prior to phagocytosis. DLS measurements of AuNPs with a FIB-BS-$T_{120}W_3$ PC in water support this, showing a higher degree of agglomeration in comparison to the AuNP–corona complexes in this work. TEM images for AuNP cell uptake after 16 hours show a significantly lower number of AuNPs inside cells for all AuNP–corona complexes (Fig. S6†).

Overall, in this work we show that the PC of AuNPs is significantly affected by incubation time in BS. Specific layers of proteins are removed upon washing revealing proteins with different electrostatic characteristics and an increase in the number of proteins with pI > 7. The number of washing steps influences particle agglomeration with AuNPs de-agglomerating after the third wash. Evidence from SERS and proteomics analysis suggest that prolonged incubation time (T_{120}) leads to an interchange of proteins in the hard PC of AuNPs with a higher amount of cationic proteins. The phenylalanine band in the SERS spectra of AuNPs–BS particles is readily visible despite repeated washing steps and may be used in future studies to quantify the amount of BSA present in the PC.

TEM images of the PC support scattering studies by SAXS that suggest the hard PC to be approximately 1.8 nm in thickness for AuNPs-BS-$T_{120}W_3$. This is in contrast to the PC produced when the particles are incubated with the protein FIB

instead, with a thickness of 3.175 nm estimated from SAXS modelling. This PC is likely to interact with the gold surface side-on, as evidenced from TEM images. FIB polypeptide chains are linked by 29 inter- and intra-chain disulphide bonds that play role in the interaction with the gold surface.[24,25] A combined AuNP-FIB-BS corona was formed which showed a distinctively different PC morphology. Large fibres (>100 nm in length and diameter) are visible resembling those formed after FIB self-assembly following thrombin activation (see also Fig. S9† for additional images).[26] A significant increase in agglomeration of AuNPs is additionally observed from DLS measurements (Fig. S5(a)†). Interestingly, the SERS spectra of AuNP-FIB-BS and AuNP-BS-FIB shows some subtle differences: bands at 1500, 1072, 1032 and 643 cm^{-1} associated with AuNP-FIB are only observed in the spectra of AuNP-BS-FIB indicating an enrichment of FIB content in this corona.

Whilst cell viability in BV2 microglia remains high for all samples, the amount of intracellular oxidative stress induced by the AuNPs with difference PC varies. The AuNP-FIB PC induces the highest level of oxidative stress. FIB is well known to induce activation of microglia, especially when immobilised, *via* the Mac-1 receptor.[25,27] Surprisingly, when the combined AuNP-FIB-BS hard corona is incubated in microglia, a synergistic effect is observed whereby the ROS(+) cells decreases despite an increase in cellular uptake. We postulate that a phagocytic uptake mechanism is promoted by the larger particle agglomeration.

When the order of incubation is reversed, *i.e.* an initial incubation for in BS followed by FIB (AuNP-BS-FIB) the high particle uptake is retained, albeit with a further decrease in ROS(+) cells, similar to negative controls (Fig. S7†).

Conclusions

The composition and properties of the soft and hard corona of AuNPs *via* a combination of scattering and microscopy techniques is reported. Noticeable differences in protein composition and hydrodynamic particle size are observed suggestive of a selective removal of protein layers. It is possible to detect changes in the composition of the PC from the SERS spectra of the BS incubated and washed AuNPs. However, quantitative proteomics data, using for example sequential window acquisition of all theoretical fragment ion spectra mass spectrometry (SWATH-MS) is necessary to correlate these changes to specific proteins in the corona.

A FIB hard corona is prepared which results in different morphology of the AuNP–corona complex. Evidence from SAXS data in combination with TEM images suggest a side-on binding of FIB. The formation of a sequential PC combining a pre-incubation in FIB followed by incubation in BS was also produced, which showed a contrast pattern indicative of a different morphology.

The cell uptake of AuNPs was largely affected by the type of corona complex formed prior to incubation in microglia. This also affected the ability of the particles to generate intracellular oxidative stress. A hard FIB-BS-corona complex showed double the cell uptake over 24 hours, with a significant decrease in oxidative stress. This effect may be due to an increase in particle agglomeration, evident from DLS, promoting a phagocytic uptake mechanism.

In conclusion, a promising approach to control cell uptake and oxidative stress of AuNPs is demonstrated *via* the selective formation of AuNP–corona complexes after removal of the soft PC.

Conflicts of interest

There are no conflicts to declare.

Acknowledgements

We are extremely grateful for funding from the Australia's Nuclear Science and Technology Organisation for access to the Australian Synchrotron (AS183/SAXS/14099). We would like to acknowledge the help of Dr Tim Ryan with sample preparation and analysis at the SAXS beamline of the Australian Synchrotron. This work was also financed through support from the ARC Centre of Excellence for Nanoscale BioPhotonics (CE140100003), an ARC Future Fellowship (AEGB, FT150100342), as well as a Macquarie University Infrastructure grant (MQRIBG-9201501951). This research has been facilitated by access to Australian Proteome Analysis Facility (APAF, Macquarie University) which is funded by an initiative of the Australian Government as part of the National Collaborative Research Infrastructure Strategy. J. R. thanks the facilities at the Electron Microscope Unit at UNSW Sydney.

Notes and references

1 D. Docter, D. Westmeier, M. Markiewicz, S. Stolte, S. K. Knauer and R. H. Stauber, *Chem. Soc. Rev.*, 2015, **44**, 6094–6121.
2 S. Tenzer, D. Docter, J. Kuharev, A. Musyanovych, V. Fetz, R. Hecht, F. Schlenk, D. Fischer, K. Kiouptsi, C. Reinhardt, K. Landfester, H. Schild, M. Maskos, S. K. Knauer and R. H. Stauber, *Nat. Nanotechnol.*, 2013, **8**, 772–781.
3 B. Fadeel and A. E. Garcia-Bennett, *Adv. Drug Delivery Rev.*, 2010, **62**, 362–374.
4 X. Huang and M. A. El-Sayed, *J. Adv. Res.*, 2010, **1**, 13–28.
5 P. García Calavia, G. Bruce, L. Pérez-García and D. A. Russell, *Photochem. Photobiol. Sci.*, 2018, **17**, 1534–1552.
6 R. García-Álvarez, M. Hadjidemetriou, A. Sánchez-Iglesias, L. M. Liz-Marzán and K. Kostarelos, *Nanoscale*, 2018, **10**, 1256–1264.
7 M. Hadjidemetriou and K. Kostarelos, *Nat. Nanotechnol.*, 2017, **12**, 288.

8 A. M. Clemments, C. Muniesa, C. C. Landry and P. Botella, *RSC Adv.*, 2014, **4**, 29134.
9 A. E. Garcia-Bennett, A. Everest-Dass, I. Moroni, I. D. Rastogi, L. M. Parker, N. H. Packer and L. J. Brown, *J. Mater. Chem. B*, 2019, **7**, 3383–3389.
10 J. Mosquera, I. García, M. Henriksen-Lacey, G. González-Rubio and L. M. Liz-Marzán, *Chem. Mater.*, 2019, **31**, 57–61.
11 T. Winuprasith, S. Chantarak, M. Suphantharika, L. He and D. J. McClements, *J. Colloid Interface Sci.*, 2014, **426**, 333–340.
12 F. Spinozzi, G. Ceccone, P. Moretti, G. Campanella, C. Ferrero, S. Combet, I. Ojea-Jimenez and P. Ghigna, *Langmuir*, 2017, **33**, 2248–2256.
13 H. He, C. Xie and J. Ren, *Anal. Chem.*, 2008, **80**, 5951–5957.
14 A. G. Miller and J. W. Macklin, *Anal. Chem.*, 1983, **55**, 684–687.
15 V. J. C. Lin and J. L. Koenig, *Biopolymers*, 1976, **15**, 203–218.
16 G. P. Szekeres and J. Kneipp, *Front. Chem.*, 2019, **7**, 30.
17 W. H. Stein and S. Moore, *J. Biol. Chem.*, 1949, **178**, 79–91.
18 B. Fazio, C. D'Andrea, A. Foti, E. Messina, A. Irrera, M. G. Donato, V. Villari, N. Micali, O. M. Maragò and P. G. Gucciardi, *Sci. Rep.*, 2016, **6**, 26952.
19 M. A. Dobrovolskaia, A. K. Patri, J. Zheng, J. D. Clogston, N. Ayub, P. Aggarwal, B. W. Neun, J. B. Hall and S. E. McNeil, *Nanomedicine*, 2009, **5**, 106–117.
20 I. Pilz, O. Glatter and O. Kratky, *Methods Enzymol.*, 1979, **61**, 148–249.
21 S. Roy and A. K. Dasgupta, *FEBS Lett.*, 2007, **581**, 5533–5542.
22 J. Deng, M. Sun, J. Zhu and C. Gao, *Nanoscale*, 2013, **5**, 8130–8137.
23 D. Davalos, J. K. Ryu, M. Merlini, K. M. Baeten, N. Le Moan, M. A. Petersen, T. J. Deerinck, D. S. Smirnoff, C. Bedard, H. Hakozaki, S. Gonias Murray, J. B. Ling, H. Lassmann, J. L. Degen, M. H. Ellisman and K. Akassoglou, *Nat. Commun.*, 2012, **3**, 1227.
24 J.-Z. Zhang and C. Redman, *J. Biol. Chem.*, 1996, **271**, 30083–30088.
25 Z. J. Deng, M. Liang, M. Monteiro, I. Toth and R. F. Minchin, *Nat. Nanotechnol.*, 2011, **6**, 39–44.
26 D. B. Kell and E. Pretorius, *Integr. Biol.*, 2014, **6**, 486–510.
27 R. A. Adams, J. Bauer, M. J. Flick, S. L. Sikorski, T. Nuriel, H. Lassmann, J. L. Degen and K. Akassoglou, *J. Exp. Med.*, 2007, **204**, 571–582.